

# In-situ bandaged Josephson junctions for superconducting quantum processors

Alexander Bilmes,<sup>1,\*</sup> Alexander K. Händel,<sup>1</sup> Serhii Volosheniuk,<sup>2</sup> Alexey V. Ustinov,<sup>1,3,4</sup> and Jürgen Lisenfeld<sup>1</sup>

<sup>1</sup>Physikalisches Institut, Karlsruhe Institute of Technology, 76131 Karlsruhe, Germany

<sup>2</sup>Kavli Institute of Nanoscience, Delft University of Technology, 2628 CJ Delft, Netherlands

<sup>3</sup>National University of Science and Technology MISIS, Moscow 119049, Russia

<sup>4</sup>Russian Quantum Center, Skolkovo, Moscow 143025, Russia

(Dated: October 12, 2021)

**Shadow evaporation is commonly used to micro-fabricate the key element of superconducting qubits - the Josephson junction. However, in conventional two-angle deposition circuit topology, unwanted stray Josephson junctions are created which contribute to dielectric loss. So far, this could be avoided by shorting the stray junctions with a so-called bandage layer deposited in an additional lithography step, which may further contaminate the chip surface. Here, we present an improved shadow evaporation technique allowing one to fabricate sub-micrometer-sized Josephson junctions together with bandage layers in a single lithography step. We also show that junction aging is significantly reduced when junction electrodes are oxidized in an oxygen atmosphere directly after deposition.**

In superconducting quantum processors, qubits are realized with non-linear resonators formed by capacitively or inductively shunted Josephson tunnel junctions [1, 2]. It is commonly understood that dielectric loss in insulation layers and tunnel junction barriers contributes strongly to energy relaxation [3]. Even without deposited dielectrics, surface oxides and contamination at electrode interfaces are major limiting factors for qubit coherence [4–7].

Qubits require submicrometer-sized Josephson junctions to enhance the circuit’s non-linearity, and to minimize the amount of lossy dielectric in the junction’s tunnel barriers [3, 8]. Usually, such junctions are made using electron-beam patterning of photoresist to form a Dolan-bridge [9, 10], an intersection of narrow trenches [11–13], or asymmetric undercuts [14]. The shadow cast by these structures when metal is evaporated from two different angles then defines the junction area. After the junction’s bottom electrode has been deposited, it is oxidized to form the tunnel barrier, and capped by the top electrode in the second evaporation step. Typically, submicrometer-sized junctions are fabricated on top of pre-patterned larger circuit structures such as shunt capacitors, which are made with faster UV-optical lithography [15].

Since the electrodes of the qubit’s shunt capacitor are also oxidized during tunnel barrier formation, they are connected to the junction’s top electrode through unwanted additional, so-called ‘stray’ junctions. The contribution of stray junctions to the qubit Hamiltonian is made negligible when they are much larger than the qubit junctions [16]. Increasing the area of the stray junction also reduces the ac-voltage drop across them and thus limits dielectric loss due to structural defects in their tunnel barriers [17]. Nevertheless, even large stray junctions may still contribute significantly to decoherence [18].

Improved qubit coherence is obtained when stray junctions are shorted using so-called bandages that are deposited in a successive lithography step [5]. However, this requires

additional lithography which consumes time and carries the risk of introducing further contamination.

Here, we describe an improved shadow-evaporation technique to fabricate sub-micrometer-sized Dolan bridge Josephson junctions together with bandage layers in a single lithography step by using three-angle evaporation. After junction formation, an argon milling plasma [19] is applied in-situ prior to bandage deposition. Importantly, due to the anisotropy of the remote argon plasma, the sub-micrometer Josephson junction is protected in the shadow of the resist mask from damage due to impacting ions. In addition, we observe that junction aging, i.e. the drift of normal-state resistance or superconducting critical current, is significantly reduced when the junction electrodes and the bandage layers are oxidized in a controlled atmosphere directly after their deposition.

We note that a similar bandaging technique has recently been developed independently by Osman *et al.* and demonstrated for Manhattan-style Josephson junctions [20].

Figure 1a shows the double resist mask used to form in-situ bandaged Josephson junctions (ISBJ). The Dolan bridge highlighted in green defines the junction area, underneath of which the two Al-electrodes evaporated from  $\pm 24^\circ$  angles are overlapping, see Fig. 1b. Before the second deposition, the bottom electrode is oxidized in a static pressure of 15 mBar for 180s to form the tunnel barrier. Note that the narrow side trenches are oriented perpendicular to the evaporation direction of the junction electrodes, so that the underlying qubit electrodes (gray) are not exposed as shown in Fig. 1b where the mask has been omitted for clarity.

Next, ion-milling is applied in the same vacuum chamber to sputter the oxide from the Al films. Finally, the bandage is deposited (yellow in Fig. 1c) perpendicularly to the substrate to create a galvanic contact between junction layers and the qubit electrodes through the side trenches. The contact areas and the Josephson contact are indicated in the legend of the exploded view shown in the right panel of Fig. 1c. The Dolan bridge protects the junction from the argon milling and from being shorted by the bandage. An image of a dc-SQUID fabricated on sapphire, which consists of two ISBJs, is shown

\*e-Mail: abilmes@google.com

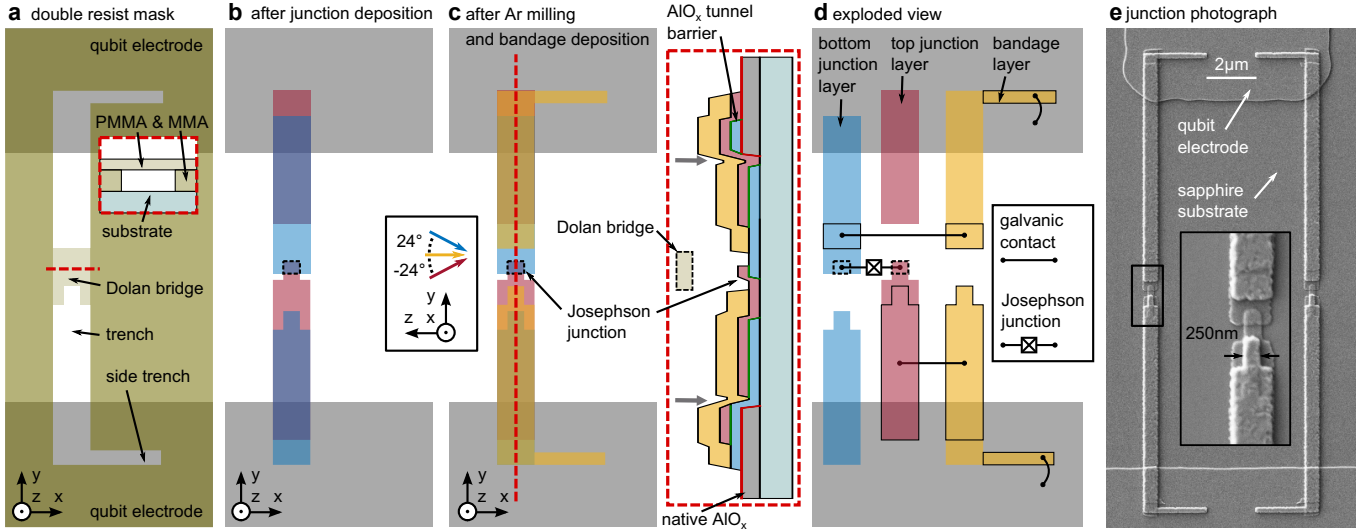


FIG. 1: **a** Sketch of the double resist mask and the Dolan bridge (see inset) for the fabrication of in-situ bandaged Josephson junctions. For clarity, the resist mask is not shown in the following sketches. **b** The Josephson junction (dashed rectangle) is created after deposition of a first (red) and second (blue) Al layers at tilted angles (see inset) and an intermediate oxidation which forms the tunnel barrier. Note that no material is deposited in the bottom of the side-trenches visible in **a**. **c** Without breaking the vacuum, the aluminum oxide is cleaned from the qubit electrodes (gray) and the junction films by argon ion milling, and a bandage film is deposited perpendicularly to the wafer. The inset shows a cross-section of the junction layers (not to scale) along the red dashed line. **d** The exploded view reveals the chain of galvanic contacts which interconnects the qubit electrodes through the Josephson contact. **e** Electron-microscopy image of a DC-SQUID consisting of two in-situ bandaged Josephson junctions, connected to the electrodes of a transmon qubit.

in Fig. 1e.

Note that the bandage spans possible discontinuities of the junction electrodes at the film edges of the qubit electrodes, which are marked in the inset of Fig. 1c by gray arrows. This simplifies the electrode geometry since no basewire hooks [5] are required which are commonly used to avoid film interruptions.

The critical current density of the junctions is calibrated from measurements of their normal resistance  $R_n$  at room temperature via the empirical relation  $E_t = E_m (R_t/R_n)^{2.5}$  [21] where  $E_m$  is the static oxidation exposure (mBar·s) during tunnel barrier formation,  $R_t$  is the target normal resistance, and  $E_t$  the adjusted oxygen exposure. However, the junction resistance typically shows temporal drift, known as junction aging [22]. To explain aging, it was suggested that the tunnel barrier might incorporate aluminum hydrates [23], where the  $\text{OH}^-$ -group may stem from organic resist residuals [24] or from water dissociation at the aluminum oxide interface [6]. It has also been shown that better long-term stability is obtained when junctions are annealed at a few hundred °C temperature in vacuum [22], which was explained by dissociation of aluminum hydrates [23].

We monitored the stability of 500 in-situ bandaged junctions (yield > 96%) by measuring their normal resistance  $R_n$  directly after fabrication and after annealing for 10 min at 200 °C in air. Junctions fabricated as described above (type A junctions) showed a resistance drop of  $(42 \pm 2)\%$  after annealing. This might be due to contamination of the junction

barrier by resist re-deposition during argon ion milling, and during lift-off in liquid stripper.

The resistance drop after junction annealing was reduced to  $(29 \pm 2)\%$  when the junctions were additionally oxidized *in-situ* after bandaging (type B junctions). Strongest improvement was observed when an additional oxidation step was applied between junction formation and subsequent argon ion milling ("protective oxidation", type C junctions), which reduced the resistance drop to  $(6 \pm 3)\%$ . We speculate that the thicker aluminum oxide may hinder contaminants from diffusing towards the tunnel barrier. Figure 2a summarizes the statistics of our observations for the three junction types.

The protective oxidation of junction electrodes also improves the long-term stability during storage. After three weeks at ambient conditions (stored in a laboratory drawer), the resistance of type B junctions increased by  $(24 \pm 6)\%$ , while type C junctions showed an increase of  $(3 \pm 3)\%$  (see Fig. 2b).

To test the suitability of in-situ bandaged Josephson junctions for quantum bits, we used them to fabricate Xmon-type transmon qubits [15, 27]. These had charge and Josephson energies designed to  $E_C \sim 200$  MHz and  $E_J \sim 20$  GHz, respectively. We monitored their energy relaxation times  $T_1$  at qubit resonance frequencies of about 6 GHz during several hours to account for temporal fluctuations due to the interference with material defects [28, 29]. Figure 3a shows histograms of  $T_1$  for two tested samples. The obtained average  $T_1$  times were very similar than those we obtained on similarly designed

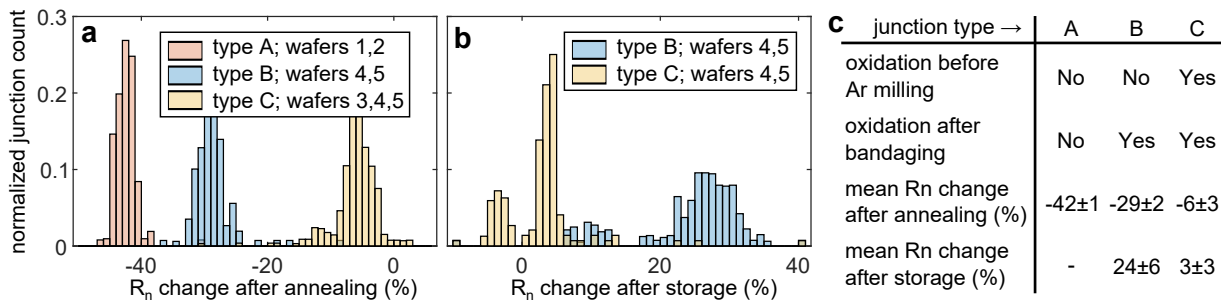


FIG. 2: **a** Resistance change of in-situ bandaged Josephson junctions after thermal annealing (10 min at 200°C in air). Type B junctions were oxidized in-situ after bandaging, while type C junctions were additionally oxidized after junction deposition (10 min at 30 mBar O<sub>2</sub>). Wafers 4 and 5 were cleaved in two after mask development. **b** Resistance change after storage for three weeks at ambient conditions. Type A junctions were not tested. **c** Overview of oxidation steps applied to each junction type, and their resistance change after annealing and storage.

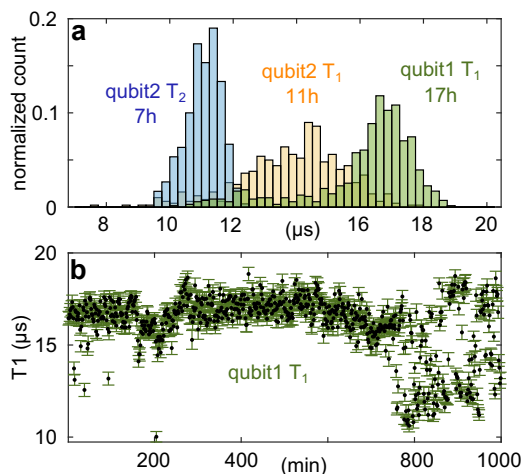


FIG. 3: **a** Histograms of energy relaxation time  $T_1$  and Ramsey dephasing time  $T_2$  recorded over several hours (the duration is indicated in each histogram label), with two out of three qubits from a same qubit chip. Qubit three was tuned far away from the Transmon sweet spot due to trapped vortices. **b**  $T_1$  records vs. time which result in the histogram for qubit No. 1 in the panel above. We recognize that the qubit experienced strong coherence fluctuations in the last three hours of records, most probably due to coupling to some charged tunneling defects [25, 26].

qubits [30] that were fabricated either with classical shadow junctions [9, 10] or cross-type junctions [12, 31]. Thus, ISBJs did not generate identifiable excess dielectric loss. Figure 3 **b** contains the time evolution of  $T_1$  of qubit No. 1, showing strong fluctuations during the last hours of measurement. This is a common issue that is explained by resonance frequency fluctuations of strongly interacting tunneling defects residing on qubit electrodes [25, 26].

We conclude that the presented technique is applicable for fabrication of coherent qubits that are free of stray Josephson junctions, and it works reliably and economizes one lithography step. The reported method also preserves the advantage of conventional bandaging [5] where the interface

of junction films to the substrate was not harmed by argon ion milling, and it is slightly simpler than the in-situ bandaging technique [20] based on Manhattan-style junctions [11], as it requires a uniaxial wafer tilt for shadow evaporation. Moreover, we observed that the changes of junction resistance induced by thermal annealing and by long-term storage are significantly reduced by adding oxidation steps after junction and bandage layer depositions.

These results offer improvements in the fabrication of stable and contamination-free Josephson junctions as required by quantum-limited parametric amplifiers [32, 33] and superconducting quantum processors. The in-situ bandaging technique to avoid parasitic tunnel barriers can also facilitate the deposition of multi-material stacks, e.g. to fabricate superconductor-ferromagnet junctions which have applications in spintronics [34] and superconducting logic circuits [35]. It is also suitable for so-called cross junctions whose bottom layer is deposited separately [8, 12], where the top and bandaging layers can be deposited under distinct wafer orientations.

#### Author Contributions

The fabrication method and design for ISBJs was developed by AB, and fabricated and tested by AB, SV and AKN. Measurements on qubits were done by JL. The manuscript was written by AB and JL with contributions from all authors.

#### Acknowledgements

The authors gratefully acknowledge funding by Google LLC, and support by the KIT-Publication Fund of the Karlsruhe Institute of Technology. AVU acknowledges partial support provided by Rosatom, and the Ministry of Education and Science of the Russian Federation in the framework of the Program to Increase Competitiveness of the NUST MISIS (contract No. K2-2020-022).

## Supplementary Material

See supplementary material for detailed fabrication recipe of the studied in-situ bandaged Josephson junctions.

## Data Availability

The data that support the findings of this study are available from the corresponding author upon reasonable request.

- 
- [1] Krantz, P. *et al.* A quantum engineer's guide to superconducting qubits. *Applied Physics Reviews* **6**, 021318 (2019). URL <https://doi.org/10.1063/1.5089550>. <https://doi.org/10.1063/1.5089550>.
- [2] Kjaergaard, M. *et al.* Superconducting qubits: Current state of play. *Annual Review of Condensed Matter Physics* **11**, 369–395 (2020).
- [3] Martinis, J. M. *et al.* Decoherence in Josephson qubits from dielectric loss. *Physical Review Letters* **95**, 210503 (2005).
- [4] Quintana, C. M. *et al.* Characterization and reduction of microfabrication-induced decoherence in superconducting quantum circuits. *Appl. Phys. Lett.* **105**, 062601 (2014). URL <http://scitation.aip.org/content/aip/journal/apl/105/6/10.1063/1.4893297>.
- [5] Dunsworth, A. *et al.* Characterization and reduction of capacitive loss induced by sub-micron Josephson junction fabrication in superconducting qubits. *Applied Physics Letters* **111**, 022601 (2017).
- [6] de Graaf, S. E. *et al.* Direct identification of dilute surface spins on  $\text{Al}_2\text{O}_3$ : Origin of flux noise in quantum circuits. *Phys. Rev. Lett.* **118**, 057703 (2017). URL <https://link.aps.org/doi/10.1103/PhysRevLett.118.057703>.
- [7] Bilmes, A. *et al.* Resolving the positions of defects in superconducting quantum bits. *Scientific Reports* **10**, 1–6 (2020).
- [8] Steffen, M. *et al.* State tomography of capacitively shunted phase qubits with high fidelity. *Phys. Rev. Lett.* **97**, 050502 (2006). URL <https://link.aps.org/doi/10.1103/PhysRevLett.97.050502>.
- [9] Niemeyer, J. & Kose, V. Observation of large dc supercurrents at nonzero voltages in Josephson tunnel junctions. *Applied Physics Letters* **29**, 380–382 (1976). URL <https://doi.org/10.1063/1.89094>. <https://doi.org/10.1063/1.89094>.
- [10] Dolan, G. J. Offset masks for lift-off photoprocessing. *Applied Physics Letters* **31**, 337–339 (1977). URL <https://doi.org/10.1063/1.89690>. <https://doi.org/10.1063/1.89690>.
- [11] Potts, A., Parker, G., Baumberg, J. & de Groot, P. CMOS compatible fabrication methods for submicron Josephson junction qubits. *IEEE Proceedings-Science, Measurement and Technology* **148**, 225–228 (2001).
- [12] Wu, X. *et al.* Overlap junctions for high coherence superconducting qubits. *Applied Physics Letters* **111**, 032602 (2017).
- [13] Kreikebaum, J., O'Brien, K., Morvan, A. & Siddiqi, I. Improving wafer-scale Josephson junction resistance variation in superconducting quantum coherent circuits. *Superconductor Science and Technology* **33**, 06LT02 (2020).
- [14] Lecocq, F. *et al.* Junction fabrication by shadow evaporation without a suspended bridge. *Nanotechnology* **22**, 315302 (2011).
- [15] Barends, R. *et al.* Coherent Josephson qubit suitable for scalable quantum integrated circuits. *Phys. Rev. Lett.* **111**, 080502 (2013).
- [16] Stehli, A. *et al.* Coherent superconducting qubits from a subtractive junction fabrication process. *Applied Physics Letters* **117**, 124005 (2020). URL <https://doi.org/10.1063/5.0023533>. <https://doi.org/10.1063/5.0023533>.
- [17] Müller, C., Cole, J. H. & Lisenfeld, J. Towards understanding two-level-systems in amorphous solids: insights from quantum circuits. *Reports on Progress in Physics* **82**, 124501 (2019).
- [18] Lisenfeld, J. *et al.* Electric field spectroscopy of material defects in transmon qubits. *npj Quantum Information* **5**, 1–6 (2019).
- [19] Grünhaupt, L. *et al.* An argon ion beam milling process for native AlOx layers enabling coherent superconducting contacts. *Applied Physics Letters* **111**, 072601 (2017). URL <https://doi.org/10.1063/1.4990491>. <https://doi.org/10.1063/1.4990491>.
- [20] Osman, A. *et al.* Simplified Josephson-junction fabrication process for reproducibly high-performance superconducting qubits. *Applied Physics Letters* **118**, 064002 (2021). URL <https://doi.org/10.1063/5.0037093>. <https://doi.org/10.1063/5.0037093>.
- [21] Kleinsasser, A. W., Miller, R. E. & Mallison, W. H. Dependence of critical current density on oxygen exposure in Nb-AlO<sub>x</sub>/Nb tunnel junctions. *IEEE Transactions on Applied Superconductivity* **5**, 26–30 (1995).
- [22] Koppinen, P., Väistö, L. & Maasilta, I. Complete stabilization and improvement of the characteristics of tunnel junctions by thermal annealing. *Applied Physics Letters* **90**, 053503 (2007).
- [23] Gates, J., Washington, M. & Gurvitch, M. Critical current uniformity and stability of Nb/Al-oxide-Nb Josephson junctions. *Journal of Applied Physics* **55**, 1419–1421 (1984).
- [24] Pop, I.-M. *et al.* Fabrication of stable and reproducible submicron tunnel junctions. *Journal of Vacuum Science & Technology B, Nanotechnology and Microelectronics: Materials, Processing, Measurement, and Phenomena* **30**, 010607 (2012).
- [25] Klimov, P. V. *et al.* Fluctuations of energy-relaxation times in superconducting qubits. *Phys. Rev. Lett.* **121**, 090502 (2018). URL <https://link.aps.org/doi/10.1103/PhysRevLett.121.090502>.
- [26] Schlör, S. *et al.* Correlating decoherence in transmon qubits: Low frequency noise by single fluctuators. *Phys. Rev. Lett.* **123**, 190502 (2019). URL <https://link.aps.org/doi/10.1103/PhysRevLett.123.190502>.
- [27] Koch, J. *et al.* Charge-insensitive qubit design derived from the Cooper pair box. *Physical Review A* **76**, 042319 (2007).
- [28] Müller, C., Cole, J. H. & Lisenfeld, J. Towards understanding two-level-systems in amorphous solids: insights from quantum circuits. *Reports on Progress in Physics* **82**, 124501 (2019). URL <https://doi.org/10.1088/1361-6633/ab3a7e>.
- [29] Burnett, J. J. *et al.* Decoherence benchmarking of superconducting qubits. *npj Quantum Information* **5**, 54 (2019). URL <https://doi.org/10.1038/s41534-019-0168-5>.
- [30] Bilmes, A., Volosheniuk, S., Ustinov, A. V. & Lisenfeld, J. Probing defect densities at the edges and inside Josephson junctions of superconducting qubits (2021). 2108.06555.
- [31] Steffen, M. *et al.* State tomography of capacitively shunted phase qubits with high fidelity. *Phys. Rev. Lett.* **97**, 050502 (2006). URL <http://link.aps.org/doi/10.1103/PhysRevLett.97.050502>.
- [32] Sweeny, M. & Mahler, R. A travelling-wave parametric amplifier utilizing Josephson junctions. *IEEE Transactions on Magnetics* **21**, 654–655 (1985).
- [33] Macklin, C. *et al.* A near-quantum-limited Josephson traveling-

- wave parametric amplifier. *Science* **350**, 307–310 (2015).
- [34] Linder, J. & Robinson, J. W. Superconducting spintronics. *Nature Physics* **11**, 307–315 (2015).
- [35] Feofanov, A. *et al.* Implementation of superconductor/ferromagnet/superconductor  $\pi$ -shifters in superconducting digital and quantum circuits. *Nature Physics* **6**, 593–597 (2010).
- [36] Rooks, M. J. *et al.* Low stress development of poly(methylmethacrylate) for high aspect ratio structures. *Journal of Vacuum Science & Technology B: Microelectronics and Nanometer Structures Processing, Measurement, and Phenomena* **20**, 2937–2941 (2002). URL <https://avs.scitation.org/doi/abs/10.1116/1.1524971>.  
<https://avs.scitation.org/doi/pdf/10.1116/1.1524971>.

# In-situ bandaged Josephson junctions for superconducting quantum processors

## Supplementary Material

### A. SAMPLE FABRICATION

#### Wafer preparation and optical lithography

The 3", C-plane, DSP, 500um sapphire wafer was washed in piranha solution and then cleaned in a barrel asher (10 min, 45 sccm O<sub>2</sub>, 150 W, 0.7 mbar). Loaded into the vacuum chamber of a PLASSYS evaporation tool, the wafer was baked for 2 hours at 200°C, then cooled down over night (~ 12h). Further, a gentle O<sub>2</sub>/Ar cleaning plasma was applied for 10s with a Kaufmann source, and after successive Titanium gettering, 100nm of aluminum were evaporated (at 1 nm/s) to form the ground plane.

The large structures (transmission line, resonators, qubit electrodes) with a critical dimension of 2.5 μm were patterned into the Al film with an Ar-Cl inductively coupled plasma, using an S1805 resist mask which was prepared in an optical lithography step.

#### Formation of the Josephson junctions

An MMA/PMMA double resist mask with a critical dimension of 250nm was prepared in an electron-beam lithography. After development of the mask, the PMMA residuals were removed in the barrel asher (3 min, 8 sccm O<sub>2</sub>, 270 W, 0.6 mbar), after which the wafer was loaded into the PLASSYS and pumped to a loadlock pressure of 3e-7mbar. After a short plasma cleaning and Titanium gettering as described above, the ISBJ is formed. The film thicknesses of the first and second junction electrodes were 30nm each while the bandage was 140nm thick.

#### Detailed fabrication steps

Three junction types (A,B and C) were studied which differ by extra oxidation steps before and after bandaging, as described below.

#### 1. Wafer preparation (3"):

- (a) Clean with piranha solution (mix of sulfuric acid H<sub>2</sub>SO<sub>4</sub> and hydrogen peroxide H<sub>2</sub>O<sub>2</sub>) to remove organic residuals.
- (b) Oxygen plasma clean in the "barrel asher" (see Tab I): 10 min duration, 45 sccm O<sub>2</sub> at a chamber pressure of 0.7 mBar, 150W generator power.
- (c) After the O<sub>2</sub> clean, transfer (~ 5 min) the wafer into the PLASSYS shadow evaporator and pump the load lock for 2h at 200°C. Cool down to room temperature over night. Final pressure is ~ 1 · 10<sup>-7</sup> mBar.
- (d) Apply oxygen-argon cleaning recipe (Table II) for 10 sec at 45° tilt angle.
- (e) Ti gettering (deposit ~ 30nm Ti into the load lock with closed shutter, and wait for 5 min).
- (f) Deposit ~ 100nm Al that will define the qubit ground plane (zero tilt, deposition rate of 1 nm/s).
- (g) Apply static oxidation (10 min at 30 mBar) to passivate the Al film surface.
- (h) Store the wafer at ambient conditions for at least one hour to stabilize the native oxide of the Al film.
- (i) Spin coat the wafer with S1818 protecting resist, and dice it into seven 2 cm × 2 cm wafers.
- (j) Remove the protecting resist in a NEP bath (1 h at 90°C).

#### 2. Definition of qubit electrodes and readout resonator:

- (a) Spin coat the wafer (2 cm × 2 cm) with S1805 resist (~ 300nm thick, 6k rpm, 60 sec, 1 min on hotplate at 115 °C), and apply positive optical lithography using the mask aligner (Tab. I).
- (b) Etch the Al film using an Ar-Cl plasma in an ICP device (Tab. I).
- (c) Remove the resist in a NEP bath (1 h at 90°C).

#### 3. Deposition of the in-situ bandaged Josephson junctions:

- (a) Spin coat the wafer with a double resist (~ 250nm PMMA A-4 on top of ~ 900nm MMA EL-13, each spun at 2k rpm for 100 sec, and baked for 5 min at 200°C), and cover with a thin Gold film to improve electric conductivity in the following positive electron-beam lithography step (JEOL device, see Tab. I). Develop the mask in a cold Isopropanol/water mixture (3/2) at 6°C [36].
- (b) Oxygen plasma clean with the barrel asher (3 min duration, 7.5 sccm O<sub>2</sub>, 230W generator power) to remove resist residuals.
- (c) Load the wafer into the PLASSYS and pump the load lock for ~ 2h at room temperature to a pressure of ~ 4 · 10<sup>-7</sup> mBar.

- (d) Apply oxygen-argon recipe (Table II) for 5 sec at 50° tilt, in order to clean the wafer underneath the Dolan bridge of the resist mask.
  - (e) Ti gettering.
  - (f) Deposit 30nm Aluminum at 24°, and at a rate of 1 nm/s, in order to define the junction's bottom electrode.
  - (g) Apply static oxidation (exposure 180s at 15 mBar) to form the AlO<sub>x</sub> tunnel barrier.
  - (h) Deposit 30nm Aluminum at -24°, and at a rate of 1 nm/s, to form the junction's top electrode.
  - (i) For junction type C, apply a static oxidation (10 min at 30 mBar) to passivate the junction's surface, and protect it from contamination during in-situ bandaging.
  - (j) Apply argon milling (Table III) for 2.5 min at zero tilt, in order to remove the oxide from the junction electrodes, and native oxide from the qubit electrodes.
  - (k) Deposit 140nm Aluminum at zero tilt, to define the bandage which galvanically interconnects all junction layers and the qubit electrodes.
  - (l) For junction type B and C, apply a static oxidation (10 min at 30 mBar) to passivate the junction's surface, and protect it from contamination during liftoff.
  - (m) Lift-off in a NEP bath (1 h at 90°C).
4. dicing into small chips, as described in 1i.

Device	Model
electron beam writer	JEOL JBX-5500ZD 50keV acceleration voltage
mask aligner	Carl Sues MA6, Xe 500 W lamp, wave lengths: 240, 365, 405 nm
inductively coupled plasma (ICP) device	Oxford Plasma Technology Plasmalab 100 ICP180 variable substrate temp. 273 – 343 K
shadow evaporation device	PLASSYS MEB550s
O <sub>2</sub> cleaner ("Barrel asher")	"nano", Diener electronic GmbH 40kHz generator, 0 – 300 W

TABLE I: Apparatus used at KIT to fabricate qubit samples.

<b>Descum</b> (10 sccm O <sub>2</sub> , 5 sccm Ar)				
Cathode	Discharge	Beam	acceleration	neutralizer
8 V	40 V	50 V	11 V	5 V (emission)
5 A	0.1 A	5 mA	4 mA	9 V 11 mA

TABLE II: Parameters of the KSC 1202 power supply unit that controls the KDC 40 ion source to generate the remote Oxygen-Argon plasma used to descum or clean samples in the PLASSYS MEB550s shadow evaporation tool.

<b>Argon ion-milling</b> (4 sccm Ar)				
Cathode	Discharge	Beam	acceleration	neutralizer
7 V	50 V	400 V	91 V	15 V (emission)
4 A	0.1 A	15 mA	0.9 mA	9 V 1 mA

TABLE III: Parameters of the KSC 1202 power supply unit that controls the KDC 40 ion source to generate the Argon ion-milling remote plasma in the PLASSYS MEB550s shadow evaporation device.